Imperial College London

Multi-Purpose Open-Source and Low-Cost Seismic Sensing

EEFIT Research Grant Scheme 2018

Institution of Structural Engineers

Project Report
June 2019

M. A. Bravo-Haro and A. Y. Elghazouli

Department of Civil and Environmental Engineering

Imperial College London

Table of Contents

List of Figures

List of Tables

Executive Summary

This report has been prepared for The Earthquake Engineering Field Investigation Team (EEFIT) of the Institution of Structural Engineers, as part of the EEFIT Research Grant Scheme 2018.

By taking advantage of the progress in Micro Electro-Mechanical Systems (MEMS), a low-cost sensing system for recording accelerations has been assembled and assessed in this report. This study is in agreement with the EEFIT aims and objectives, since it enables the collection of strong motion data at ground level during earthquakes, as well as monitoring of structures. It enhances the fulfilment of several key goals of EEFIT. From assessing structural performance of buildings to contributing to decision-making in earthquake-affected regions based on the actual state of critical structures and infrastructure.

The sensing technique described in this report has been entirely built from off-the-shelf electronic components, and its construction and programming guidelines will be provided as an open-source platform which will be continuously updated. The preliminary assessments carried out in this investigation suggest that the proposed sensor is suitable for deployment as an accelerograph for seismic monitoring of structural systems. The results show low levels of self-noise, considering the nature of the MEMS analogue accelerometer embedded in the sensor. The amplitude transfer functions exhibit a flat behaviour for the full range of frequencies tested, whose boundaries were limited by the installed capacity within the laboratory. However, this flat behaviour is expected to be coherent up to the resonant frequency of the MEMS accelerometer, whose absolute value is much higher than the bandwidth of frequencies of interest for seismologists and structural earthquake engineers. The clipping tests indicate a flat behaviour, i.e. high linearity, of the amplitude transfer function from low acceleration levels, up to the vicinity of the maximum nominal recordable acceleration of ± 3g, at which a typical roll-off is observed. Under long-time operations, the sensor exhibits a robust performance, maintaining a steady pace of sampling. The performance can be further refined under additional dynamic tests considering non-stationary signals, such as ground motion recordings from actual earthquakes, and potentially through comparison through intensity measure parameters from recorded data commonly used in earthquake engineering.

Overall, the work carried out within this study opens the door for several future prospects and further natural developments of this type of sensing techniques, towards obtaining a standalone real-time data collection sensor.

1. Introduction

The ever-increasing precision and ever-decreasing cost of Micro Electro-Mechanical Systems (MEMS), especially MEMS accelerometers, have enabled their implementation in a variety of industrial and scientific fields, serving a wide range of tasks that were usually solved by traditionally expensive and large devices. In the realm of seismology and earthquake engineering, MEMS accelerometers, able to record ground accelerations produced by earthquakes, have resulted in several prototypes of low-cost sensors and subsequent arrangement of seismic networks completely based on MEMS sensors. This has been recently referred to as a 'revolution in seismic detection technology' (**Cochran 2018**) that may transform earthquake science due to the affordability of the sensors themselves and the maintenance of a network of this nature, among others. Early experiences include 'The Quake-Catcher Network' where MEMS accelerometers, able to detect vibrations within $0.1 - 20$ Hz and accelerations usually within ± 2g, behave as a strong-motion seismic station (**Clayton et al. 2012; Cochran et al. 2009**). Another similar network is the 'Home Seismometer for Earthquake Early Warnings', initiated by the Japan Meteorological Agency, where a tri-axial in-house MEMS sensor is used, able to record ground accelerations within a range of ± 2g at 500 Hz (i.e., 500 samples per second) (**Horiuchi et al. 2009**). More recent examples include 'The Palert Network of Taiwan' for early earthquake warning, whose MEMS sensors record ground accelerations within ± 2g at 100 samples per second (**Wu 2015**). The first European Urban Seismic Network was developed in Acireale, Italy (**D'Alessandro 2016**), in addition to pioneering local arrays of accelerographs developed in Lefkadas, Greece (**Karakostas et al. 2018**). It is also worth noting the exploration of MEMS accelerometers embedded in smartphones, either used as fixed sensors, as in the USGS project for earthquake and tsunami early warning system deployed in Chile (**Brooks et al. 2016**), or as freely moving devices where human-induced sources of acceleration such as walking, are identified and removed from quake-induced accelerations powered by machine learning methods (**Kong et al. 2016**). Ultimately, the performance of a Raspberry Shake 4D low-cost seismograph and accelerometer (**Christensen and Blanco Chia 2017**) was recently shown to be good enough to use as a sensor to densify regional networks designed for studies of local and regional events (**Anthony et al. 2018**). Therefore, as discussed above, the potential of MEMS accelerometers for the measurement of ground motion induced by earthquakes has been demonstrated and documented internationally.

In parallel, some efforts have been made on exploring and properly documenting the use of sensors based on MEMS accelerometers in civil structures, where the nature of the vibrations is the same as in the case of ground motion. Nonetheless, several differences need to be accounted for, including the range of the amplitude of the accelerations being one of the most significant. For instance, the Community Seismic Network (**Clayton et al. 2012**) has been instrumenting buildings in California, USA, using the same sensor described above initially designed to record free-field strong-motion at the ground level. The low-cost of the sensors and their maintenance have enabled unprecedented dense arrays in tall buildings, when compared to existing instrumented buildings (e.g., **Çelebi 2006; Kohler et al. 2007**). Moreover, sensors based on MEMS accelerometers have been developed in Structural Health Monitoring (SHM), for tracking various structural typologies and sorting different needs, such as in bridges (**Bedon et al. 2018; Sabato 2015; Sekiya et al. 2016; Zhou and Yi 2013**); and powered by different sensors (**Holovatyy et al. 2017; Pakzad et al. 2008; Ruiz-Sandoval et al. 2006**).

In order to illustrate some key aspects that differentiate the peak ground acceleration (PGA) and the response acceleration of a structure, **Figure 1** shows the 5%-damped elastic response spectra of two recordings from recent earthquakes in Chile (2010) and Mexico (2017), respectively. The response spectrum is a fundamental concept in Earthquake Engineering, which provides a summary of the peak response of all possible linear single-degree-of-freedom systems when subjected to a particular component of ground motion (**Biot 1932**). It can be observed here that the maximum acceleration experienced by a wide range of structural systems (i.e., different periods of vibration), is significantly higher than the PGA (i.e., period equal to zero), normally recorded by strong-motion seismic stations. In spite of the deeply dissimilar characteristics of both recordings, in terms of seismogenesis and soil conditions, it is interesting to observe the ratios between the peak acceleration experienced by the structure and the PGA, whose values attain 5.10 and 5.31 for the Maule and Puebla recordings respectively, for a 5%-damped spectral response. Therefore, when significant values of PGA are recorded, as for instance, in the case of

the Maule Earthquake recording (**Figure 1**a) whose PGA is equal to 0.697g, a building might undergo a peak acceleration of 3.549g, if the fundamental period of vibration is tuned to 0.17s. This level of acceleration is typically higher than the maximum range or clipping level of existing MEMS accelerometers or strong-motion seismic stations. In addition, it is important to mention that strength reduction factors are frequently applied to the elastic spectrum, and therefore lower accelerations are considered for structural design, mostly due to the inelastic deformations allowed in the structural system much earlier than the yield elastic limit. However, focusing the attention in the peak structural response exhibited by the roof of a multi-storey building, response accelerations 18 times higher than the PGA might be attained (**Miranda et al. 2018**), therefore even higher ratios with respect to the PGA in the case of sensitive non-structural elements that are placed in the floor.

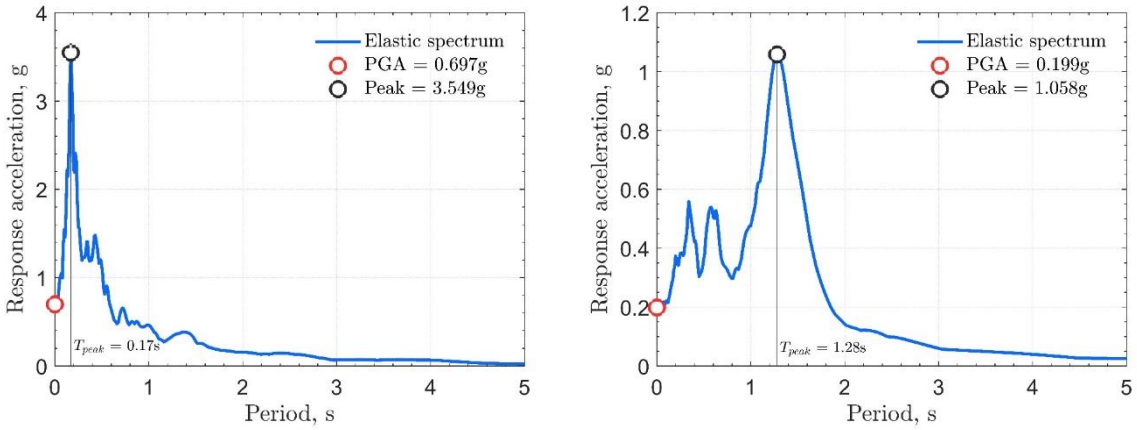

(a) (b)

Figure 1. (a) Elastic response spectrum from the 2010 Maule Earthquake in Chile, $M_w = 8.8$, channel 1, Angol station. (b) Elastic response spectrum from the 2017 Puebla Earthquake in Mexico, $M_w = 7.1$, channel 1, JC54 station. Damping ratio equal to 0.05 for both spectra.

This report presents a preliminary assessment of the performance of a low-cost accelerograph, built with off-the-shelf electronic components. This is executed throughout standard tests and metrics commonly employed to evaluate the performance of sensors for measuring vibrations, such as seismographs (**ANSS 2008**). Promising results are shown regarding the capabilities of the sensor to be used as an accelerograph in structural systems, based on the low self-noise, high acceleration sensitivity, and robustness in long-term operation. Importantly, the maximum recordable acceleration or clip level of the sensor is higher than ± 3g with a well-behaved clipping of the signal in the time space. However, further tests on the maximum capacity of the sensor are still needed due to laboratory equipment limitations as discussed below. Finally, some insights on a secondary stage of development of the sensor are drawn, towards real-time data collection, connectivity, power supply possibilities, and general maintenance of a full operational sensor.

This study is in agreement with the EEFIT aims and objectives, since it enables the collection of strong motion data at ground level during earthquakes, as well as monitoring of structures. It enhances the fulfilment of several key goals of EEFIT. From assessing structural performance of buildings to contributing to decision-making in earthquake-affected regions based on the actual state of critical structures and infrastructure.

2. Methodology

In order to enable the use of a sensor as a reliable recorder of induced accelerations, it is central to understand the behaviour of the final configuration of the device, which usually comprises a MEMS accelerometer attached to a Micro-Controller or to a small Motherboard, in addition to wiring, batteries, and frequently another kind of attached sensor in order to collect other type of information (e.g., humidity, temperature). For this type of sensors, individual characterisations are recommended to be carried out, given that sensors with identical off-the-shelf electronic components, produced by the same manufacturer, may exhibit different performance (**D'Alessandro et**

al. 2017). This variability has rarely been taken into account in the case of MEMS sensors, and only for specific aspects, such as the self-noise.

To characterise the actual performance of an accelerograph based on a MEMS accelerometer, standardised tests are undertaken, as listed below:

1. Self-noise test, to determine the lowest limit of accelerations that the sensor is capable of recording under normal conditions.
2. Box flip test, to estimate the sensitivity of the sensor.
3. Dynamic sine waveform inputs, to build amplitude transfer functions.
4. Dynamic sine waveform inputs, to determine the highest bound of acceleration, or clipping levels besides sensor linearity.
5. Single and double integration test to recover mostly transient time-histories of velocity and displacement.

Dynamic tests were performed using a linear servo-controlled actuator, by attaching the sensors to the head of the jack. In addition, for these dynamic tests, a high-accuracy commercial accelerometer (model: PCB ICP 393B04) was used to obtain an individual reference of the output signal of the actuator. This is a crucial standard practice that besides ascertaining the actual response of the mechanical system used for the tests, it helps to identify external sources of mechanically-induced noise. As shown further below, the linear actuator used for the tests, inputs some extra mechanical noise, in addition to some poor behaviour in the closed-loop feedback of the control system, mostly at the peaks of the sine wave, for high levels of induced acceleration. Hence, the maximum reliable frequency attained by the linear actuator was 17 Hz, for sine waves with low amplitudes, so that this limit defines the maximum frequency tested and used for the construction of the amplitude transfers functions of the sensor.

3. Characteristics of the Sensor

This report presents only one prototyped sensor configuration, based on an open-source Arduino UNO microcontroller and a 3-axis analogue MEMS Adafruit accelerometer ADXL 335. This arrangement of elements has been selected due to its simplicity and robustness compared to several other prototypes tested during this study. The simplicity can be appreciated in **Figure 2** where a schematic configuration of the sensor is drawn, and the robustness is judged by several factors, such as the quality of the recorded data due to the timestamp stability of the sampling, the steady uninterrupted continuous operation during long-time recording tests as presented further in detail. Interestingly, there are other configurations that may offer powerful capabilities to a sensor of this nature, that certainly need a closer look in the future. An exemplary case is the use of a Raspberry Pi single-board micro-computer, that offers the whole environment of an operating systems, among peripheral ports and embedded sensors, such as LAN and/or wireless connectivity for transferring recorded data. A Raspberry Pi can be used in replacement of an Arduino board, or jointly in order to exploit the micro-controller quality of the latter and hence reducing the overheads in the Raspberry. This was found to be crucial when a Raspberry Pi is used as a single data-acquisition system instead of an Arduino board, restricting the sampling rate of recording of the 3 axis in parallel to only 100 samples per second. In addition, several MEMS accelerometer options were tested as well, given the wide range of off-the-shelf low-cost available devices. Here, the most significant difference rests on the analogue or digital nature of the sensor. In the latter case, such as the digital ADXL 326 MEMS accelerometer explored within the study, the analogue-to-digital converter is embedded in the accelerometer and allows different pre-defined ranges of maximum recordable acceleration, up to ± 16g, where the sensitivity drops as the acceleration range increases. Nevertheless, the Arduino board capability of recording 10 bits analogue data, individually per each axis of a MEMS device, played in favour of the prototype selected for this report. Besides, the micro-controller nature of the sensor enables the execution of loops and feedback loops with a high level of precision, making it suitable as a digitizer.

For this prototype, various levels of sampling rates were considered, where the sought performance is the stability of the timestamp at each recorded sample or, in other words, the differential of time between consecutive samples

has to tend to zero. In addition, this needs to hold true for longer windows of time, where usually the final timestamp is lagged due to the accumulation of the error. This is of the greatest importance in order to record reasonable waveform and thus avoid distortions in the spectral analyses. It was found that the Arduino board is capable of recording three input channels at 400 samples per second, plus a timestamp mark. It is interesting to note that if only one axis of the accelerometer is plugged, 1000 samples per second can be attained with a robust performance. However, the capability of recording 3-axis at the same time is appealing for a sensor as this, coupled with the fact that the range of frequencies of interest is much lower than the Nyquist frequency of the rates just mentioned above. As a result, the recorded accelerations during the tests undertaken for this report are fixed at a rate of 200 samples per second. In contrast, the commercial transducer used to contrast and validate the results is fixed at a rate of 1000 samples per second, due to the capacity of the sensor and the data acquisition system used to handle it (i.e., National Instruments NI-9234 vibration input mode). Finally, **Figure 3** shows a modified configuration of the sensor that was used during the tests in order to facilitate the data acquisition process, in addition to offering access to the microcontroller during the tests. As shown in the figure, the MEMS accelerometer is wired and encased out of the box to be attached to the linear actuator.

Table 1. MEMS accelerometer nominal characteristics

Parameter	*Nominal value*
Nominal Maximum acceleration	±3g
Bandwidth for X and Y axis	1600 Hz
Bandwidth for Z axis	550 Hz
Acceleration sensitivity	300 mV/g
Noise Density X and Y axis	150 µg/√Hz rms
Noise Density Z axis	300 µg/√Hz rms
Sensor Resonant Frequency	5.5 kHz

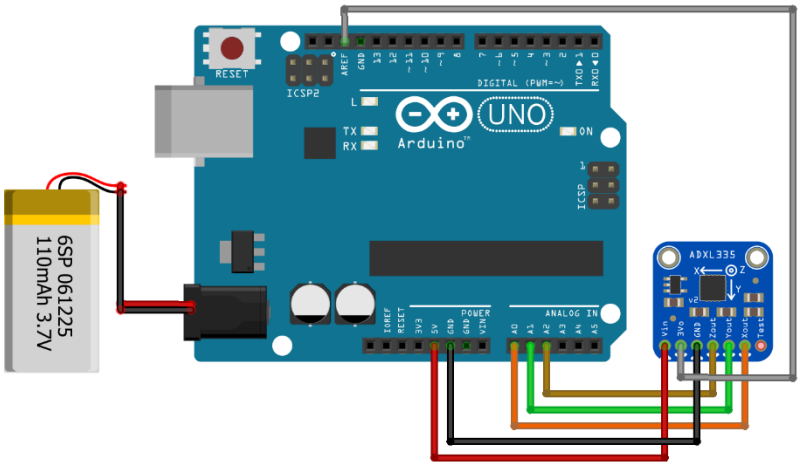

Figure 2. Schematic configuration of the sensor and general wiring between the Arduino board and the MEMS accelerometer.

Figure 3. Sensor configuration used during the tests to facilitate the collection of data and final experimental setup.

4. Performance of the Prototyped Sensor

4.1. Sensor Self-noise

The level of inherent noise produced by the sensor enables the estimation of the weakest motion signal that can be recorded by the device (**Rodgers 1992**). Input accelerations below this threshold are not recorded by the sensor, and the ones with similar amplitudes to the self-noise level are poorly recorded (**Anthony et al. 2018**), hindering the task of isolating both sources apart. There are several methods to quantify the self-noise of a sensor, yet for this report the Power Spectral Density (PSD) method is selected, along with the measurement of some individual parameters that represent the level of self-noise, such as the Constant Bias (CB).

CB or offset of the sensor in a particular axis, can be estimated as the average of a signal recorded through a long window of time under no excitation of the sensor, or zero frequency. The mean CB of the 12 hours recording for each individual axis are: $0.180\ \mathrm{m/s^2}$, $0.088\ \mathrm{m/s^2}$, and $0.118\ \mathrm{m/s^2}$ for X, Y, and Z axis, respectively. Correspondingly, the standard deviation per axis are: $1.441 \times 10^{-3}\ \mathrm{m/s^2}$, $2.848 \times 10^{-3}\ \mathrm{m/s^2}$, and $3.087 \times 10^{-3}\ \mathrm{m/s^2}$ for X, Y, and Z axis, respectively. It is important to note that the measured CB in all axis is steady trough time, and no irregular trends or time-dependant increasing CB values are observed, enabling the removal or detrend of these permanent offsets to calibrate the sensor. An excerpt of the 12 hours test recorded data is shown in **Figure 4** for all 3-axes of the accelerometer.

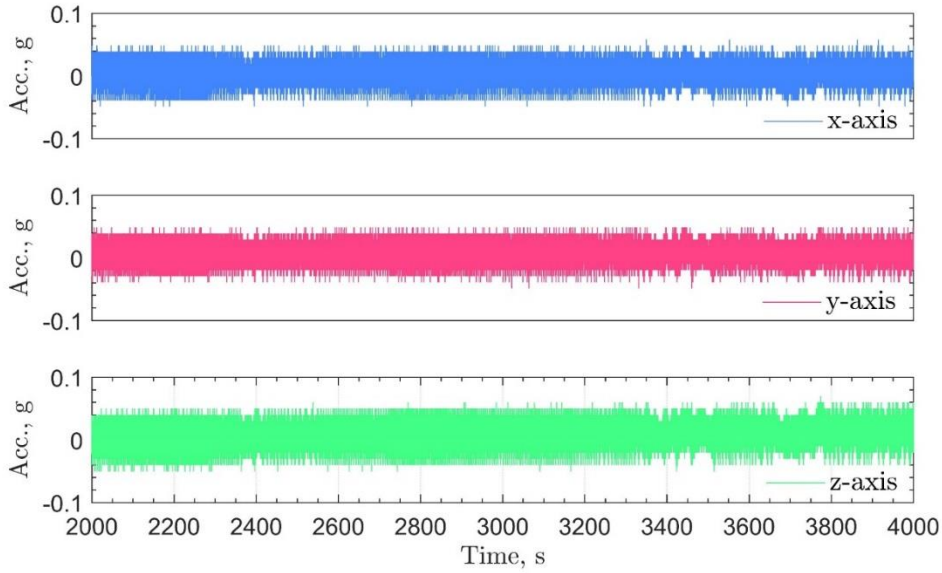

Figure 4. Excerpt of a 12 hours continuous recording under no excitation of the sensor, for all three axes of the MEMS accelerometer.

The PSD curves are shown in **Figure 5**, along with the RMS nominal self-noise density level reported by the manufacturer of the MEMS ADXL 335. Coherent with the specifications of the accelerometer, axes X and Y, report a lower level of self-noise with respect to axis Z. However, this trend remains valid for the bandwidth of frequencies lower than 1.0 Hz, since for higher frequencies, all levels of noise tend to converge towards the lowest level. Nevertheless, in the relevant bandwidth of frequencies for earthquake engineering ($\sim 0.2s - 20s$), the three axes show a relatively low self-noise PSD with respect to signals produced by even moderate earthquakes (i.e., good signal-to-noise ratio), hence enabling signal recording (**Clinton and Heaton 2002; D'Alessandro et al. 2017**).

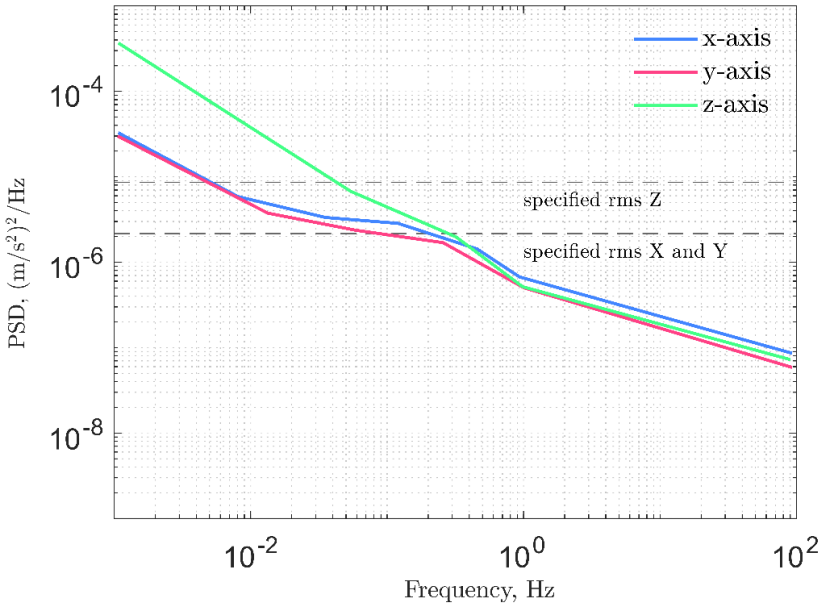

Figure 5. Power spectral density of the acceleration recorded through 12 hours of motionless state of the sensor, for every axis of MEMS accelerometer

4.2. Box-flip tests

To appraise the sensitivity of the sensor, a box-flip test was carried out. Herein, the sensor is accommodated in a cubic box in such a way that the direction of axis of the MEMS accelerometer are parallel to the edges of the box. This enables flipping of the box in turn through the 6 possible positions, in order to use the Earth acceleration gravity as a reference for all axis in the upward and downward orientation. Theoretically, this method allows estimation of the static sensitivity, offset, and orientation of every axis, along with potential accumulated drifts once the box is set to the initial position (**Evans et al. 2014**). Commonly, a measure of the Earth's static field (e.g., by using an absolute gravimeter) is used as a reference to estimate the difference with the values recorded by the sensor. However, as this accurate measure is missing at the laboratory, a referential value of g equal to 9.806 m/s^2 is used herein and the test is repeated 10 times, in order to assess the variability of recorded values.

Figure 6 shows a full sequence of one of the box-flip tests. Sequentially from left to right, the orientation of the sensor is shown for the static position in the top plot. The perturbations of the signal in between static position are due to the transient movement of the box to attain the next position. A median of the values recorded during the zero movement window, bounded by the dashed vertical lines, was used to compute the sensitivity and variability of the sensor. Additionally, negligible drifts are observed at the end of the sequence with respect to the initial measure at the beginning of the test. The latter is crucial to accurately retrieve displacements through double-integration of the acceleration recording, as shown and discussed in Section 5.

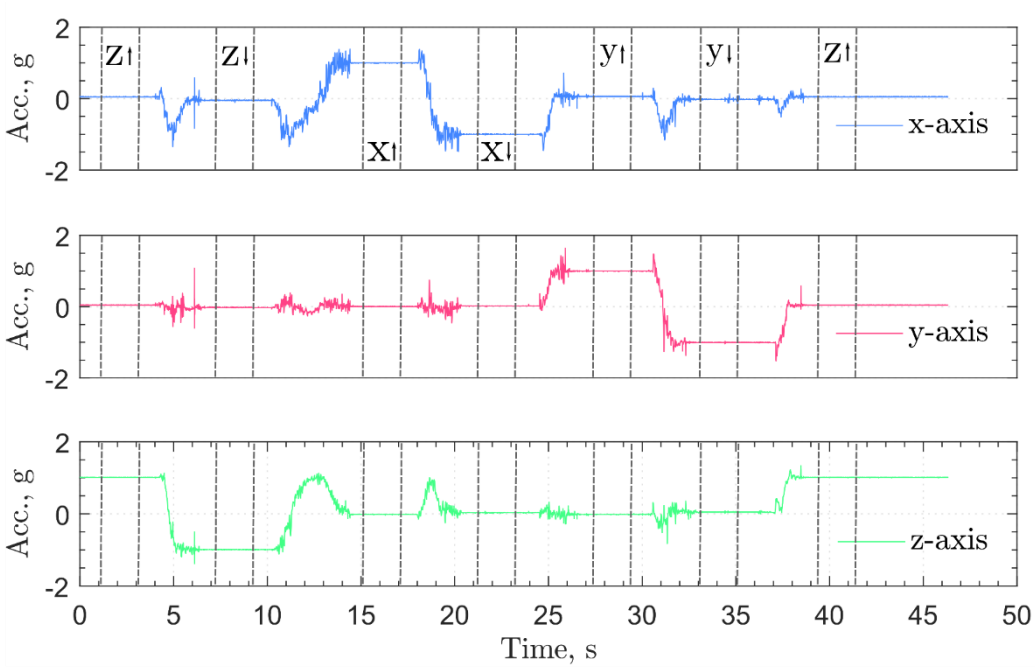

Figure 6. Flip box test based on raw data recorded by the sensor. The sequence of positions of the sensor during the test are shown at the top plot, where the arrow indicates the upward and downward position of the axis with respect to a flat surface.

4.3. Transfer function tests

A transfer function is the ratio of the output of the system to the input of the system. In this case, it relates the amplitude and the phase of the input signal given to the dynamic jack to that recorded by the sensor. The attention is herein focused on estimating the ratio of the amplitude response for a wide range of signals with different frequencies, in order to establish the range of "flat-response'' of the sensor. Towards this aim, a uniaxial dynamic

actuator was used to input sinusoidal waves with several amplitudes and frequencies, which were recorded at the same time by the MEMS sensor and the transducer. As mentioned above, the input signal (i.e. ideal synthetic signal) followed by the control system of the dynamic actuator, differs from the end actual performance of the jack, hence the information recorded by the high fidelity transducer is used as a reference in the forthcoming analyses.

The computation of the amplitude ratios can be performed directly on the time-domain by a root-mean-square (RMS) of the recorded accelerations, or it can be carried out on the frequency-domain through a spectral analysis. The main shortcoming of the former one is the sensitivity of the RMS to noise from different sources that is captured by the sensor (**Evans et al. 2014**), especially in the case of low frequency weak signal, that demand the maximum length of the actuator's stroke to achieve a minimum level of excitation in terms of acceleration, thus external and internal noise is overcome. The latter spectral method is instead used in this study due to its robustness and accuracy, and also because the recording sampling rate of the sensor is highly steady enabling frequency-domain analyses. The methodology presented by **Evans et al. 2014** is followed to compute the total power of the dominant frequencies of the signal. This is illustrated in **Figure 7** and **Figure 8** for a sine wave input with 10mm and 5Hz of nominal amplitude and frequency respectively.

Figure 7 shows an excerpt of the measured acceleration by the MEMS sensor and the transducer, in addition to the synthetic input signal, whose total response, of approximately 20 s of duration, is then used in the spectral analysis presented in **Figure 8**. The power of the signal is computed in a narrow band around the peak of the dominant frequency which for the case of the sensor usually matches the reference input frequency; this enables filtering-out the noise carried by frequencies out of the limits of the narrow band. To define this band, the highest 5 peaks reported by the sensor are used, and their FFT amplitudes are employed to render a unique acceleration value through the root-mean square method.

Before discussing the amplitude ratios obtained from all wave sine input signals considered in the test, it is worth noting that the sampling ratio of the sensor is fixed to 200 samples per seconds, whereas the transducer is sampling at 1000 samples per second, given the capability of the DAQ system reported above. By using the raw data of the transducer, a very precise match of the synthetic sine wave input to the actuator is attained, as shown in **Figure 8**.

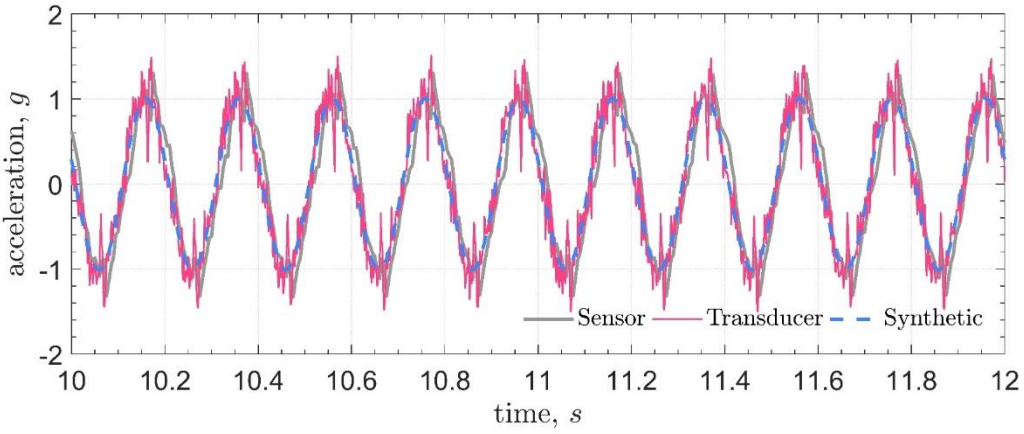

Figure 7. Excerpt of raw data from a sinusoidal input signal of 10 mm nominal amplitude and 5 Hz nominal frequency.

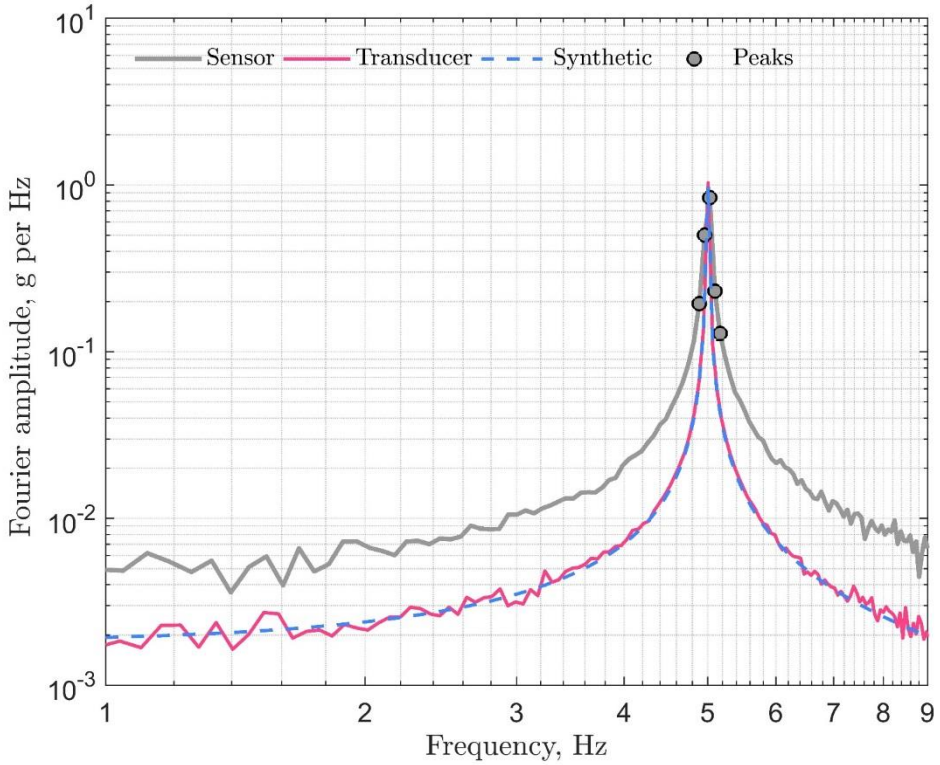

Figure 8. Fast Fourier Transform (FFT), displaying a narrowband spectral response window of a sinusoidal signal of 10 mm nominal amplitude, and 5 Hz nominal frequency. The frequency measured by the sensor is 5.002 Hz.

By computing the amplitude ratios, using the spectral method, for all input signals tested in the linear actuator, the amplitude frequency response of the sensor can be obtained, as shown in **Figure 9**, for all axes of the MEMS accelerometer. In general, the amplitude ratio shows a good behaviour, given the flatness of the amplitude response for the whole range of tested frequencies, which were limited by the mechanical capacity of the linear actuator. It is interesting to highlight the adequate behaviour of the sensor for capturing the amplitude of the input signal, either in the range of low frequencies (i.e., < 1 Hz) and in the higher range, without shouldering below the corner frequency. This behaviour is expected in MEMS devices, given that their natural frequencies are usually much higher than the ones found in the seismic band. However, this needs to be tested individually, jointly with the data acquisition configuration. For instance, there could be analogue filtering embedded in the feedback loop, thus reducing or cutting-off the observed amplitude with respect to the reference signal (**Evans et al. 2014**).

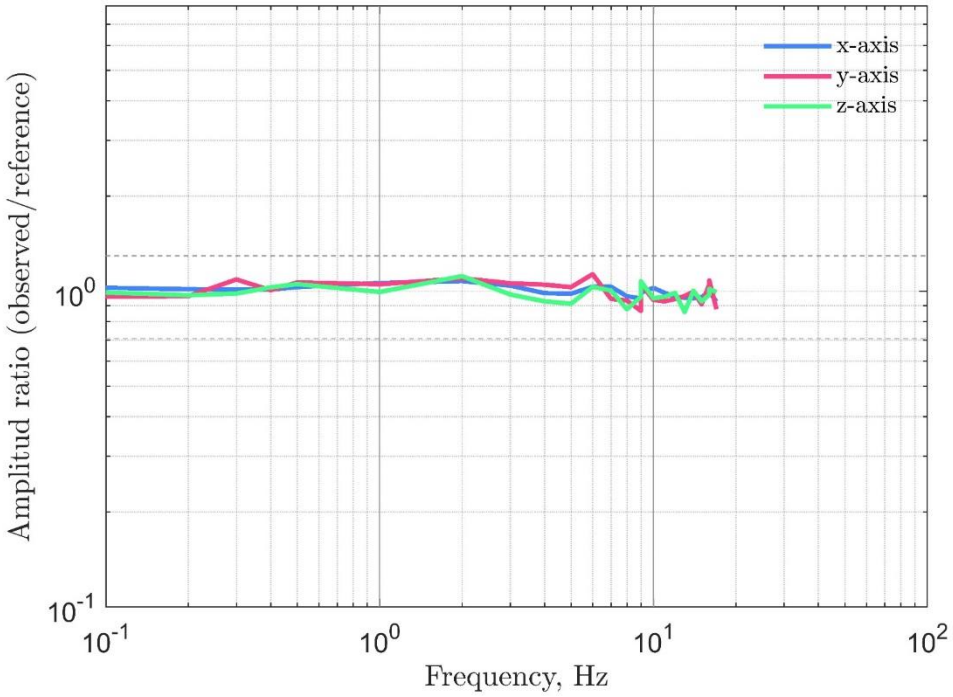

Figure 9. Computed amplitude ratios versus frequency. The high fidelity transducer is used as a signal reference instead of the synthetic signal input to the dynamic jack.

4.4. Clipping behaviour and sensor linearity

The linearity means that there is a linear relationship between input signal and output signal (**Havskov and Alguacil 2004**). The extent of sensor linearity is usually computed for a given frequency at various levels of amplitude or, in other words, a fixed frequency and variable acceleration. For sensors designed to measure strong ground-motion, a 1% of linearity is commonly accepted as a satisfactory level, as pointed out by **Havskov and Alguacil 2004**. It is interesting to note that the level of linearity is rarely specified, thus making comparison among sensors more difficult. The clipping is a form of distortion in the recorded signal with respect to input signal, once a certain threshold is surpassed. In the case of accelerometers, this threshold is commonly drawn by the mechanical capacity of the sensor, which corresponds to ± 3g for the MEMS ADXL 335 accelerometer. However, the behaviour of the distortion can vary significantly from sensor to sensor, especially in the case of MEMS as shown by **Evans et al. 2014**, where for instance, some devices actually do not clip the recorded signal but instead blow it up producing highly distorted patterns. The latter inappropriate clipping behaviour is undesirable, and may limit the capacities of the sensor; such as in the double integration processes aiming at obtaining the displacement demand from the recorded acceleration signal, as discussed below in Section 4.5.

To appraise linearity and clipping, the same methodology of inputting sine-wave signals through the linear actuator is used, and response amplitudes are estimated using spectral analysis, as discussed in the previous section. In this case, the input frequency is fixed at 9 Hz, considered to be moderate-to-high in the frequency band of interest, and the amplitude is variable in order to attain a range of acceleration ranging from 0.2g to 3.5g. The smooth clipping behaviour shown by the sensor is depicted in **Figure 10** for a sequence of increasing accelerations, around the nominal clipping level of the MEMS accelerometer, contrasted to the output signal recorded by the transducer. From **Figure 10a** to **10d**, the clipping of the sensor is pointed at the peak of the sine waves, where the sensor output signal tends to flatten whilst the transducer still captures the increase in acceleration of the input wave. By computing the amplitude ratios obtained from the tests, through the spectral method, the amplitude ratio versus acceleration levels is assembled and shown in **Figure 11**. The three axis of the

sensor clip in a well-behaved manner, as noted by **Evans et al. 2014**, given their smooth attenuation over their nominal clip threshold, that for a sine wave is commonly estimated as the RMS of the signal, which is shown in the plot with a vertical dashed line.

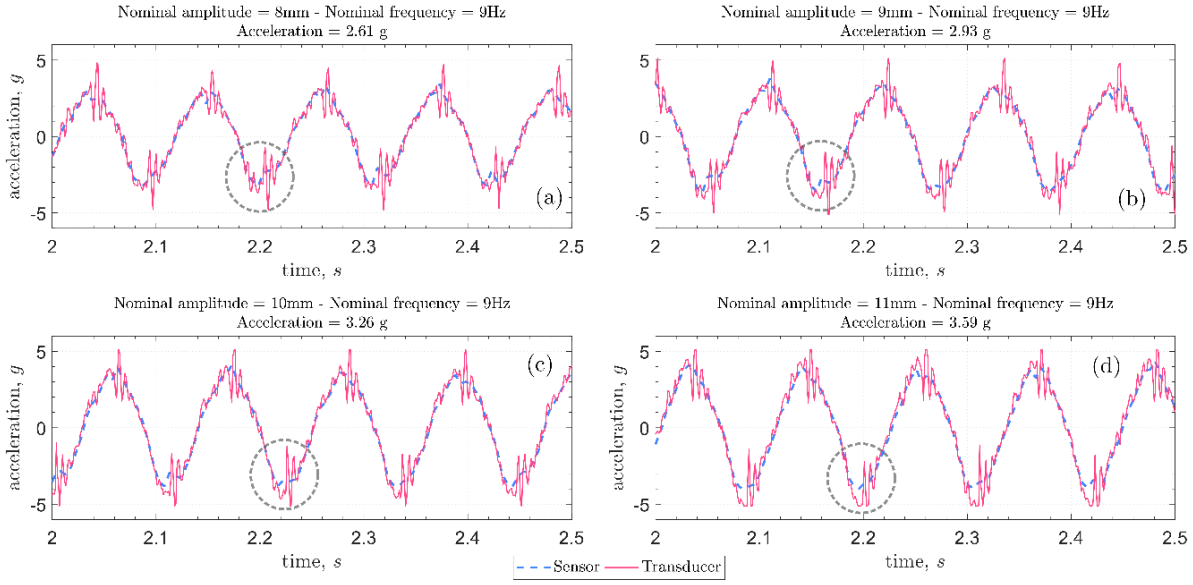

Figure 10. Sequence of tests for accelerations in the neighbourhood of the nominal clipping level of ± 3g (all excerpts of recorded data correspond to the x-axis of the sensor at fixed nominal 9Hz frequency).

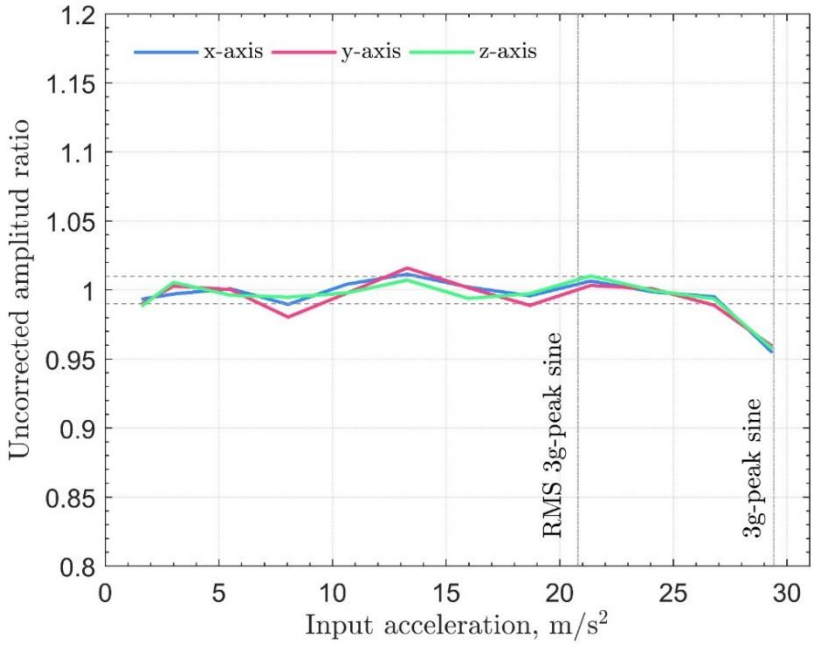

Figure 11. Linearity and clipping for the three axes of the sensor (dashed horizontal lines show $\pm 1\%$ of the expected ratio at unity).

4.5. Single and double integration tests

The capability of retrieving permanent or transient displacements from the acceleration recording is paramount during the monitoring of a building or structural system. In earthquake engineering, local drift ratios are typically the most important parameters to appraise the performance of a structure (**Çelebi 2008**), given that they can be readily related to a damage state of the system, which is usually predefined based on the structural configuration of the system. Residual or permanent drifts deserve a special attention given their crucial role in post-earthquake assessment, where structural losses are estimated, and decisions are made based on the state of the structure, such as demolition or retrofitting. (**Bravo-Haro and Elghazouli 2018; MacRae and Kawashima 1997**). Single and double integration process are commonly used to retrieve velocity and displacement time-histories from acceleration recordings, respectively. However, this is an underdetermined problem (**Evans et al. 2014**), where usually nonphysical waveforms are obtained for the velocity and displacement. The nature of these spurious results are explained partially by several sources of error, such as unknown boundary conditions for the velocity and displacement, offset of the baseline, and low-frequency noise or artifacts (**Boore and Bommer 2005; Boore et al. 2002**). Several methods have been proposed to individually remedy these sources of error, such as various baseline correction, filtering and zero-padded sections, among others; some of these are used subsequently.

The same dynamic tests using sine waves as input signals described in previous sections are used herein. Note that these test were not designed to induce residual displacements that can later be retrieved, thus the main focus here is to estimate velocity and displacement transient waveforms through time-histories. First, a baseline correction was performed through fitting a cubic polynomial function to the acceleration record, which is subsequently subtracted from the recorded acceleration. Second, zero padded sections are added to the beginning and end of the record, whose adequate length depends on the order and corner frequency of the filter to be applied afterwards (**Boore 2005**). Third, a band-pass Butterworth filter whose corner filter frequencies are 0.1 Hz and 25 Hz is applied. Finally, the acceleration record is numerically integrated to obtain the velocity and displacement time-histories. The same methodology was applied to the data collected by the transducer, in order to compare results based on the actual output of the actuator. The results of the single and double integration procedures are shown in **Figure 12**, for two different levels of nominal amplitude and frequency of the sine wave input signal. In general, step amplitudes and waveforms are well recovered by the sensor, which is an important feature in this exploratory stage, partially due to the stable sample-rate recording. It is noticeable that, for both recovered displacement time-histories, some non-steady weave behaviour occurs at the beginning of the motion, before reaching a steady state. This behaviour was initially attributed to the processing of the signal; however, the transducer coherently captured this as well, even when different processing methods were used before the integration (e.g., length of the zero-padded regions, and other filters such as Chebyshev). In addition, a similar behaviour was observed consistently for various input signal, thus explained by the control system of the actuator at the beginning of the motion, especially in the case of the highest frequencies tested. Particularly noteworthy is the fact that when residual displacement needs to be retrieved by double-integration of the acceleration record, low-cut filters cannot be used (**Evans et al. 2014**); nevertheless, this needs further consideration in the assessment of the sensor, preferably by having independently-measured offsets or residual displacements in the actual response of structural systems.

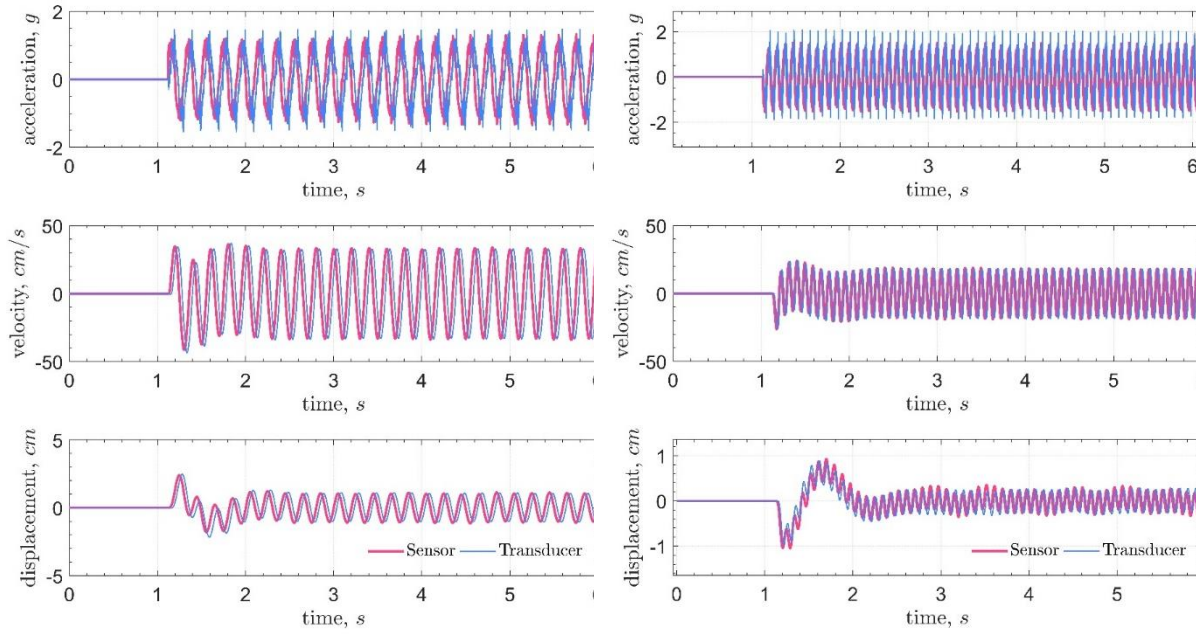

(a) (b)

Figure 12. Single and double integration test for 2 input signals: (a) Nominal amplitude = 10 mm and nominal frequency 5 Hz. (b) Nominal amplitude = 2.5mm and nominal frequency 11 Hz.

5. Further developments

Considering the results presented in this report, along with similar good performance exhibited by other MEMS-based prototypes tested, as mentioned above, the natural step forward in this research is the development of the data communication system and power supply, in order to have a standalone sensor that can be deployed in actual structural systems. In this brief final section, some ideas in this regard are presented.

One of the biggest challenges in the seismic monitoring of structures is the collection of data within a fraction of minutes or seconds after a seismic event. To achieve this, commonly there is a server at site, that collects the data from different sensors deployed in a building, then render some post-processing of collected data (e.g., down-sampling), and finally communicates the filtered and well-arranged data through the Internet to an end-user (**Çelebi et al. 2004**). Most of the times, this architecture demands expensive equipment in-situ, such as the server computer equipped with peripherals for data acquisition, extensive lines of cables between the accelerographs and the local server, among others. However, the cost impediment can be challenged if not overcome thanks to the current state and potential of microcontrollers and single-board micro-computers, where there is enough computational capacity to collect and process data into the sensor, and several communication protocols to transmit the data to the end-user side directly, without the need to have a server at site. For instance, a Raspberry Pi can get access to the internet through a wired Ethernet port (e.g., Raspberry Pi 3) or Wi-Fi (e.g., Raspberry Pi 3 and Raspberry Pi Zero). This capability is currently examined by the authors, using the single-board as digitiser and control system of MEMS accelerometers, and the collected data can be sent to a remote server in real-time. **Figure 13** shows a beta version of a web-interface for collection, processing and visualisation of data in real-time. The acceleration time-histories correspond to the tip acceleration of a cantilever scale-model under a pull-back test in the Z-direction. In addition, **Figure 14** shows the spectral density of each axis, which is calculated on the fly once the recorded acceleration data has been received in the server. The resonant frequency of the fist transversal mode is captured by the three axis, as one would expect, moreover the resonant frequency of the first longitudinal mode is captured by the longitudinal X-axis.

Currently, other protocols of communication are under exploration, as the GSM standard for digital cellular networks, available in low-cost microcontrollers such as the Arduino GSM 1400. This protocol is particularly appealing in earthquake prone regions, where Internet access is limited or simply non-existent.

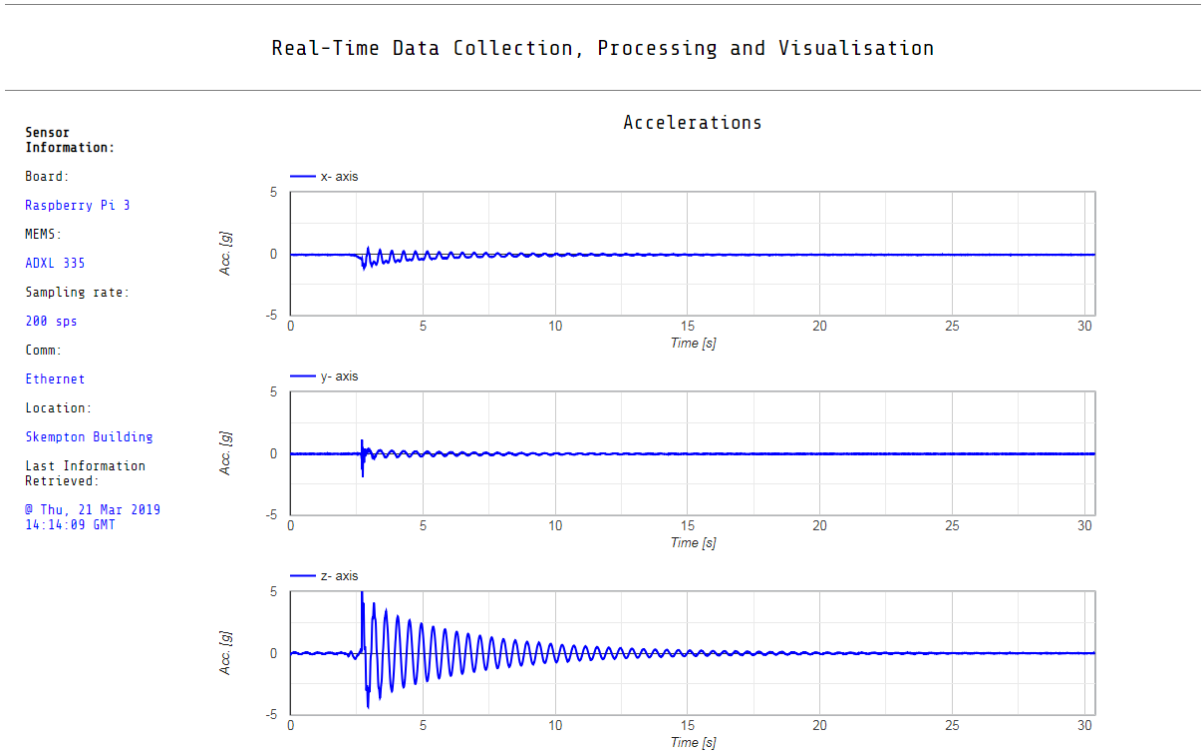

Figure 13. End-user web interface for collecting, processing and visualising acceleration data. Time-histories for all axis during the response of a cantilever pull-back in the Z-direction.

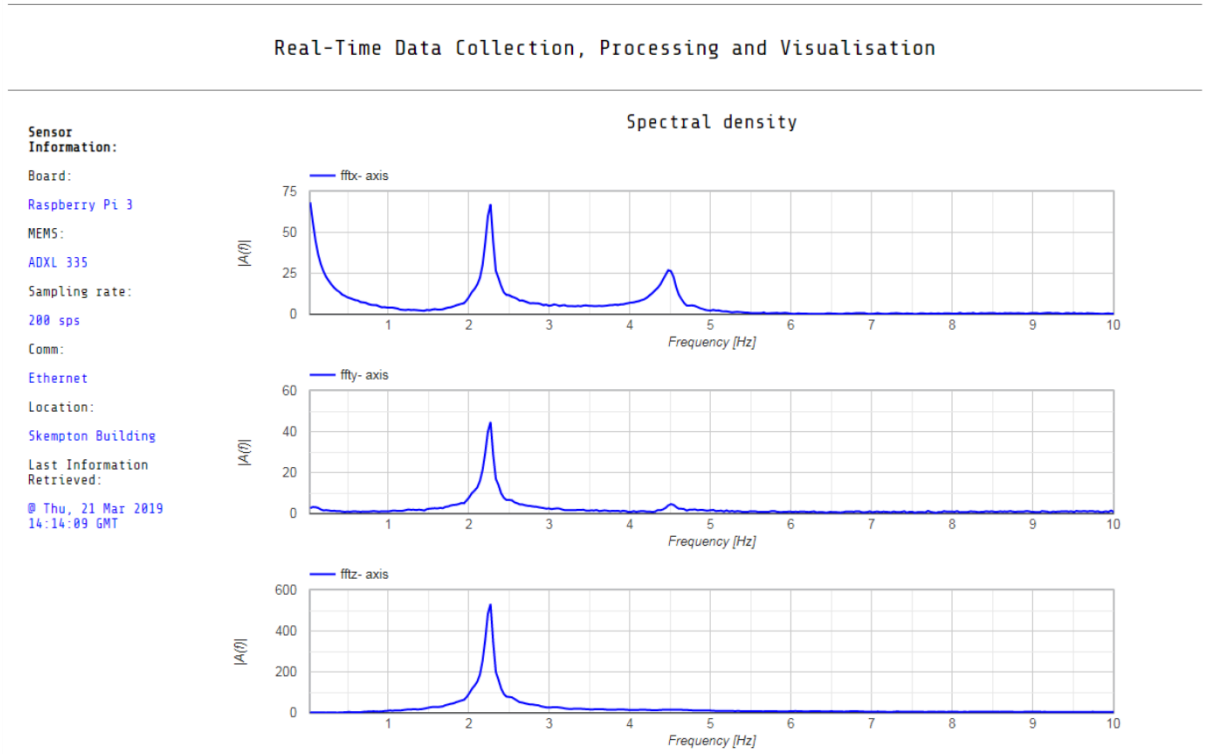

Figure 14. End-user web interface for collecting, processing and visualising acceleration data. Spectral density for all axis during the response of a cantilever pull-back in the Z-direction.

6. Concluding Remarks

A low-cost sensing system for recording accelerations has been assembled and its performance has been assessed through a series of comparative validation tests, as described in this report. The sensor has been entirely built from off-the-shelf electronic components, and its construction and programming guidelines will be provided as an open-source platform which will be continuously updated.

The assessments carried out in this investigation suggest that the proposed sensing technique is suitable for deployment as an accelerograph for seismic monitoring of structural systems. Based on standardised tests, the results demonstrate low levels of self-noise, considering the nature of the MEMS analogue accelerometer embedded in the sensor. The amplitude transfer functions exhibit a flat behaviour for the full range of frequencies tested, whose boundaries were limited by the installed capacity within the laboratory. However, this flat behaviour is expected to be coherent up to the resonant frequency of the MEMS accelerometer, whose absolute value is much higher than the bandwidth of frequencies of interest for seismologists and structural earthquake engineers. The clipping tests indicate a flat behaviour (i.e., high linearity) of the amplitude transfer function from low acceleration levels, up to the vicinity of the maximum nominal recordable acceleration of ± 3g, at which a typical roll-off is observed. Under long-time operations, the sensor exhibits a robust performance, maintaining a steady pace of sampling. Nevertheless, the performance needs to be examined further under additional dynamic tests considering non-stationary signals, such as ground motion recordings from actual earthquakes, and potentially comparison through some intensity measure parameters from recorded data commonly used in earthquake engineering.

The work carried out within this study opens the door for several future prospects and further natural developments of this type of sensing techniques, towards obtaining a standalone real-time data collection sensor. Future efforts will be focused towards the advancement in connectivity and communication protocols, power supply possibilities, and general maintenance procedures of a standalone operating sensor.

7. Acknowledgments

The support of Earthquake Engineering Field Investigation Team (EEFIT) and the Institution of Structural Engineers, through the 2018 EEFIT Research Grant Scheme, is gratefully acknowledged.

8. References

ANSS , W.G., Advanced National Seismic System., 2008. Instrumentation Guidelines for the Advanced National Seismic System [Working group on instrumentation, siting, installation, and site metadata of the Advanced National Seismic System technical integration committee]. 2008-1262.

Anthony, R.E., Ringler, A.T., Wilson, D.C. and Wolin, E., 2018. Do low-cost seismographs perform well enough for your network? An overview of laboratory tests and field observations of the OSOP Raspberry Shake 4D. Seismological Research Letters, 90(1): 219-228.

Bedon, C., Bergamo, E., Izzi, M. and Noè, S., 2018. Prototyping and validation of MEMS accelerometers for structural health monitoring—The case study of the Pietratagliata cable-stayed bridge. Journal of Sensor and Actuator Networks, 7(3): 30.

Biot, M.A., 1932. Transient oscillations in elastic systems, California Institute of Technology.

Boore, D.M., 2005. On pads and filters: Processing strong-motion data. Bulletin of the Seismological Society of America, 95(2): 745-750.

Boore, D.M. and Bommer, J.J., 2005. Processing of strong-motion accelerograms: needs, options and consequences. Soil Dynamics and Earthquake Engineering, 25(2): 93-115.

Boore, D.M., Stephens, C.D. and Joyner, W.B., 2002. Comments on baseline correction of digital strong-motion data: Examples from the 1999 Hector Mine, California, earthquake. Bulletin of the Seismological Society of America, 92(4): 1543-1560.

Bravo-Haro, M.A. and Elghazouli, A.Y., 2018. Permanent seismic drifts in steel moment frames. Journal of Constructional Steel Research, 148: 589-610.

Brooks, B., Baez, J., Ericksen, T., Barrientos, S., Minson, S., Duncan, C., Guillemot, C., Smith, D., Boese, M. and Cochran, E., 2016. Smartphone-based earthquake and tsunami early warning in Chile, AGU Fall Meeting Abstracts.

Çelebi, M., 2006. Recorded earthquake responses from the integrated seismic monitoring network of the Atwood Building, Anchorage, Alaska. Earthquake Spectra, 22(4): 847-864.

Çelebi, M., 2008. Real-time monitoring of drift for occupancy resumption, Proc. 14th World Conference on Earthquake Engineering (14WCEE).

Celebi, M., Sanli, A., Sinclair, M., Gallant, S. and Radulescu, D., 2004. Real-time seismic monitoring needs of a building owner—and the solution: a cooperative effort. Earthquake Spectra, 20(2): 333-346.

Christensen, B. and Blanco Chia, J., 2017. Raspberry Shake-A World-Wide Citizen Seismograph Network, AGU Fall Meeting Abstracts.

Clayton, R.W., Heaton, T., Chandy, M., Krause, A., Kohler, M., Bunn, J., Guy, R., Olson, M., Faulkner, M. and Cheng, M., 2012. Community seismic network. Annals of Geophysics, 54(6).

Clinton, J.F. and Heaton, T.H., 2002. Potential advantages of a strong-motion velocity meter over a strong-motion accelerometer. Seismological Research Letters, 73(3): 332-342.

Cochran, E.S., 2018. To catch a quake. Nature communications, 9(1): 2508.

Cochran, E.S., Lawrence, J.F., Christensen, C. and Jakka, R.S., 2009. The quake-catcher network: Citizen science expanding seismic horizons. Seismological Research Letters, 80(1): 26-30.

D'Alessandro, A., 2016. Tiny accelerometers create Europe's first urban seismic network. Eos, 97(10.1029).

D'Alessandro, A., Vitale, G., Scudero, S., D'Anna, R., Costanza, A., Fagiolini, A. and Greco, L., 2017. Characterization of MEMS accelerometer self-noise by means of PSD and Allan Variance analysis, 2017 7th IEEE International workshop on advances in sensors and interfaces (IWASI). IEEE, pp. 159-164.

Evans, J., Allen, R.M., Chung, A., Cochran, E., Guy, R., Hellweg, M. and Lawrence, J., 2014. Performance of several low-cost accelerometers. Seismological Research Letters, 85(1): 147-158.

Havskov, J. and Alguacil, G., 2004. Instrumentation in earthquake seismology, 358. Springer.

Holovatyy, A., Teslyuk, V., Iwaniec, M. and Mashevska, M., 2017. Development of a system for monitoring vibration accelerations based on the raspberry pi microcomputer and the adx1345 accelerometer. Eastern-European Journal of Enterprise Technologies, 6(9): 52-62.

Horiuchi, S., Horiuchi, Y., Yamamoto, S., Nakamura, H., Wu, C., Rydelek, P.A. and Kachi, M., 2009. Home seismometer for earthquake early warning. Geophysical Research Letters, 36(5).

Karakostas, C.z., Papanikolaou, V.k. and Theodoulidis, 2018., An ultra-dense strong-motion urban network based on in-house designed mems accelerographs: the case of Lefkas city, Greece. 16th European Conference on Earthquake Engineering, Thessaloniki.

Kohler, M.D., Heaton, T.H. and Bradford, S.C., 2007. Propagating waves in the steel, moment-frame factor building recorded during earthquakes. Bulletin of the Seismological Society of America, 97(4): 1334-1345.

Kong, Q., Allen, R.M., Schreier, L. and Kwon, Y.-W., 2016. MyShake: A smartphone seismic network for earthquake early warning and beyond. Science advances, 2(2): e1501055.

MacRae, G.A. and Kawashima, K., 1997. Post-earthquake residual displacements of bilinear oscillators. Earthquake engineering & structural dynamics, 26(7): 701-716.

Miranda, E., Kazantzi, A. and Vamvatsikos, D., 2018. New approach to the design of acceleration-sensitive non-structural elements in buildings, 16th European Conference on Earthquake Engineering, Thessaloniki.

Pakzad, S.N., Fenves, G.L., Kim, S. and Culler, D.E., 2008. Design and implementation of scalable wireless sensor network for structural monitoring. Journal of infrastructure systems, 14(1): 89-101.

Rodgers, P.W., 1992. Frequency limits for seismometers as determined from signal-to-noise ratios. Part 1. The electromagnetic seismometer. Bulletin of the Seismological Society of America, 82(2): 1071-1098.

Ruiz-Sandoval, M., Nagayama, T. and Spencer Jr, B., 2006. Sensor development using Berkeley Mote platform. Journal of Earthquake Engineering, 10(02): 289-309.

Sabato, A., 2015. Pedestrian bridge vibration monitoring using a wireless MEMS accelerometer board, 2015 IEEE 19th International Conference on Computer Supported Cooperative Work in Design (CSCWD). IEEE, pp. 437-442.

Sekiya, H., Kimura, K. and Miki, C., 2016. Technique for determining bridge displacement response using MEMS accelerometers. Sensors, 16(2): 257.

Wu, Y.-M., 2015. Progress on development of an earthquake early warning system using low-cost sensors. Pure and Applied Geophysics, 172(9): 2343-2351.

Zhou, G.-D. and Yi, T.-H., 2013. Recent developments on wireless sensor networks technology for bridge health monitoring. Mathematical Problems in Engineering, 2013.

Appendix A: Data used for transfer-functions test (selected)

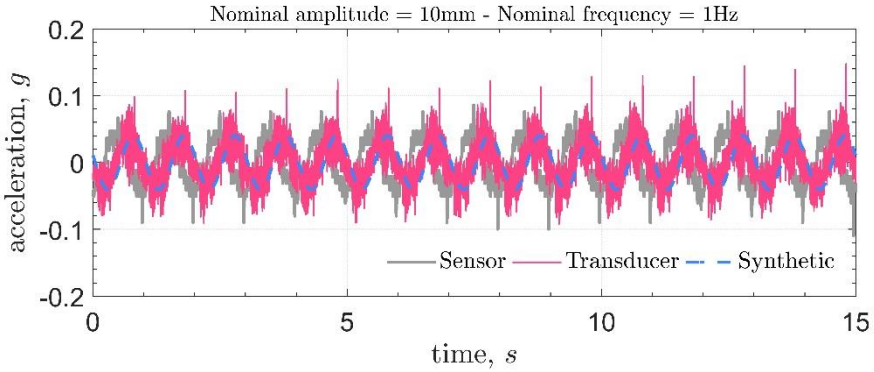

(A1)

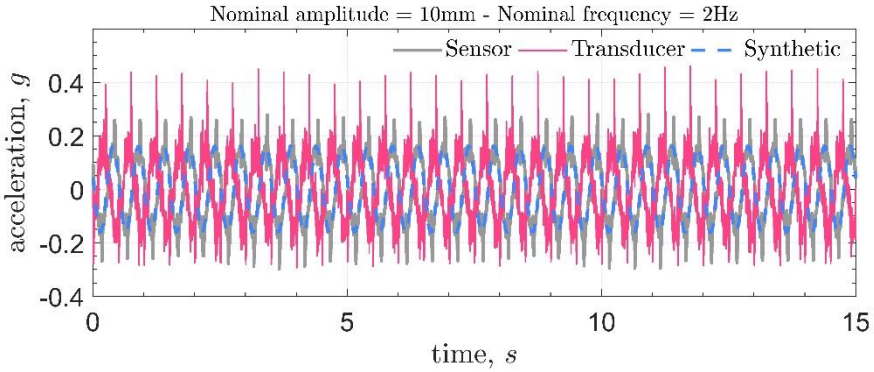

(A2)

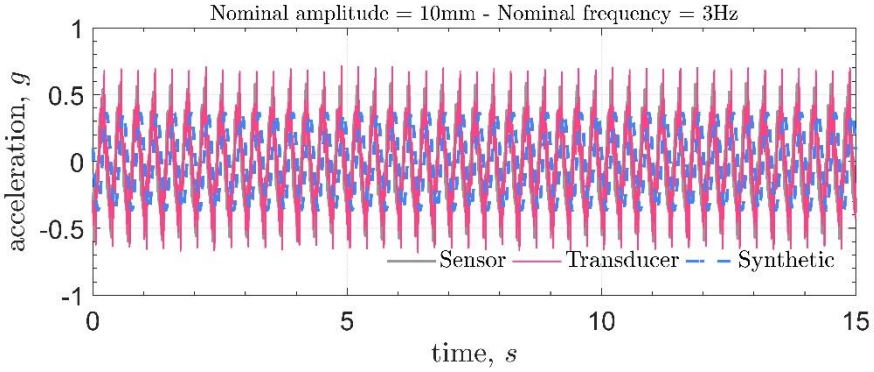

(A3)

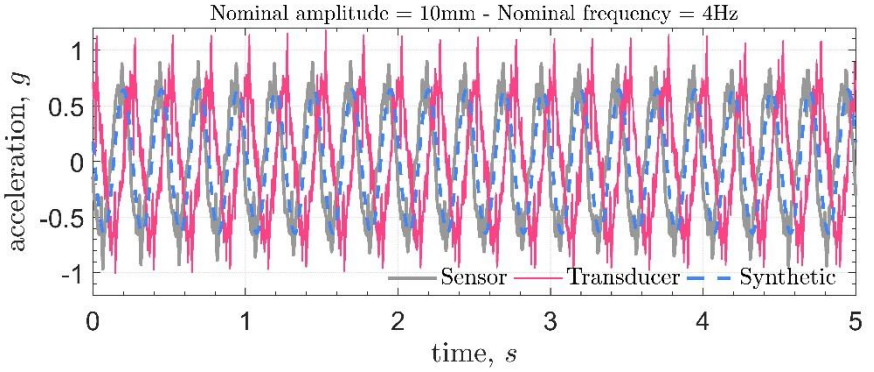

(A4)

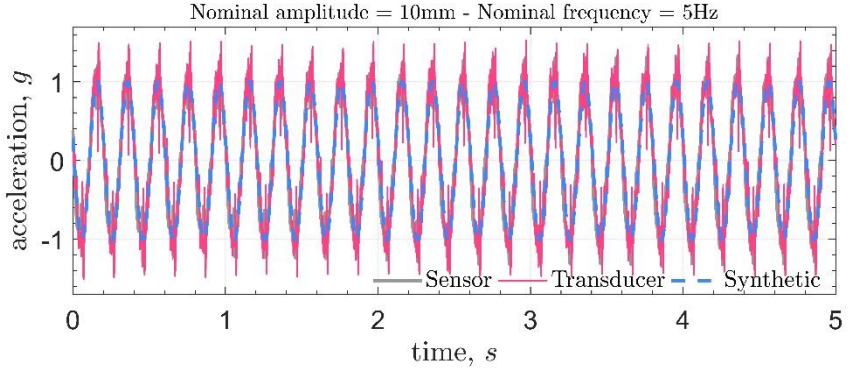

(A5)

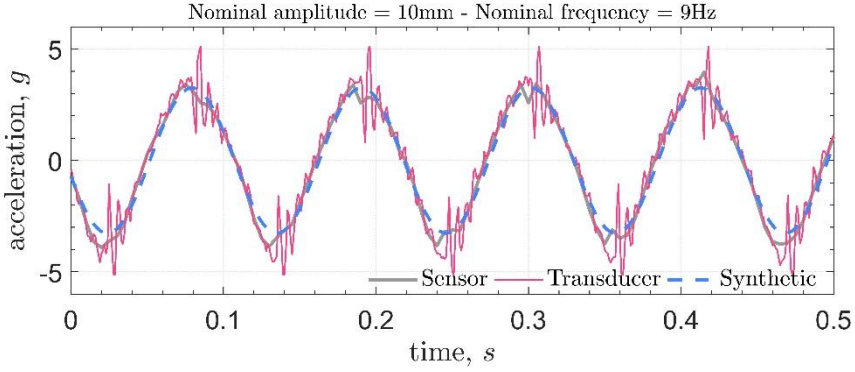

(A6)

Appendix B: Data used for clipping and linearity tests (selected)

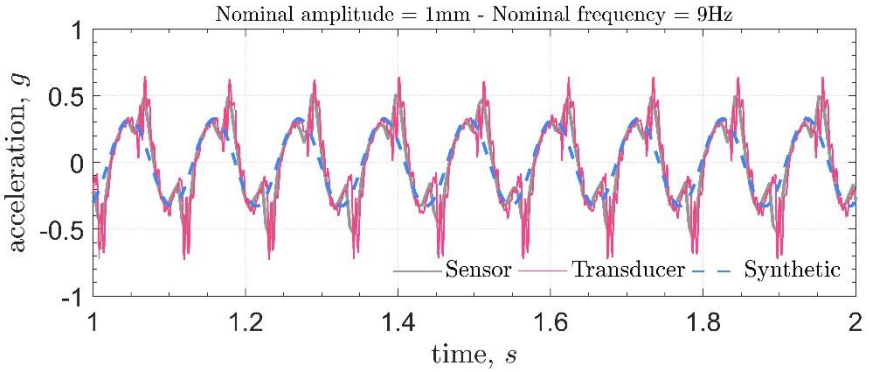

(B1)

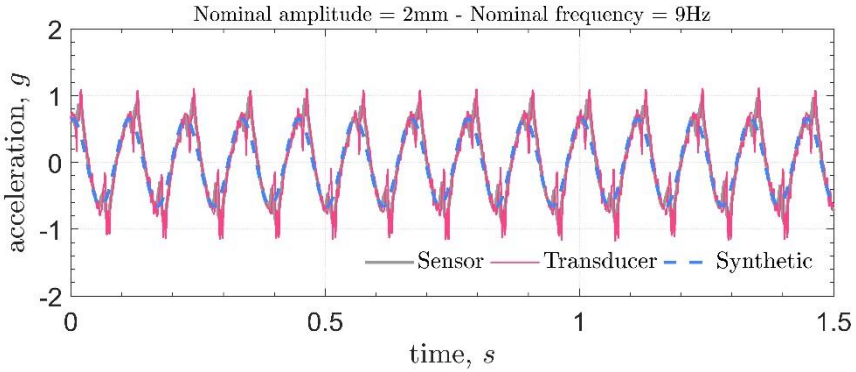

(B2)

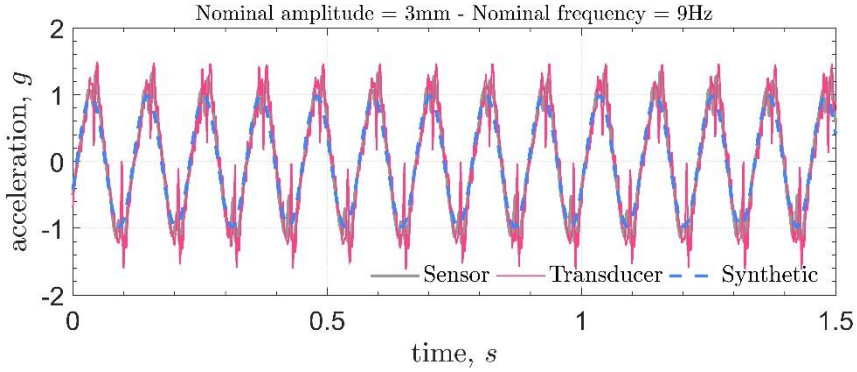

(B3)

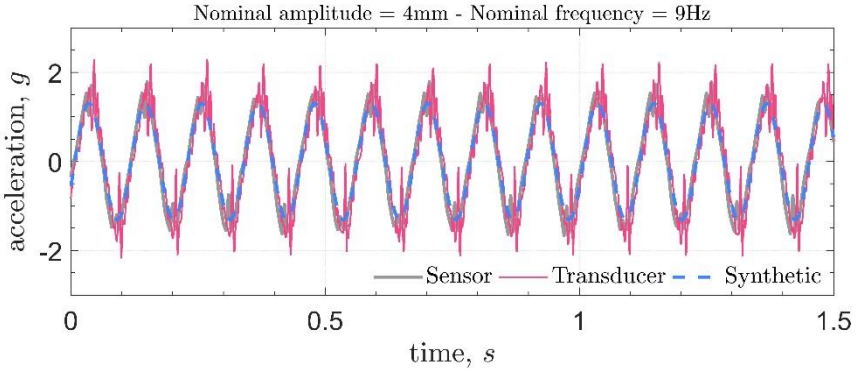

(B4)

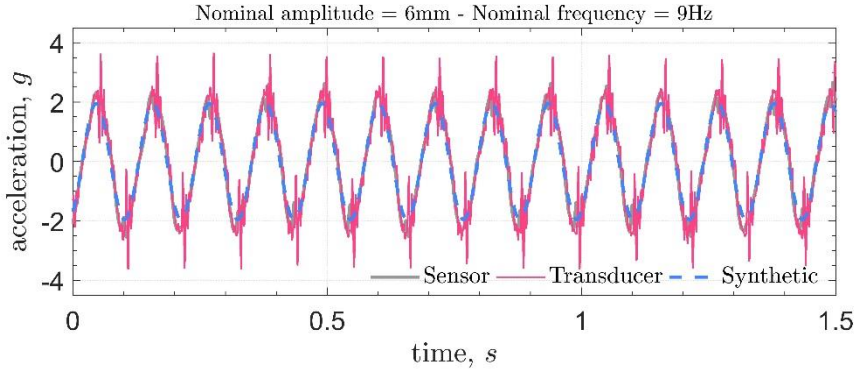

(B5)

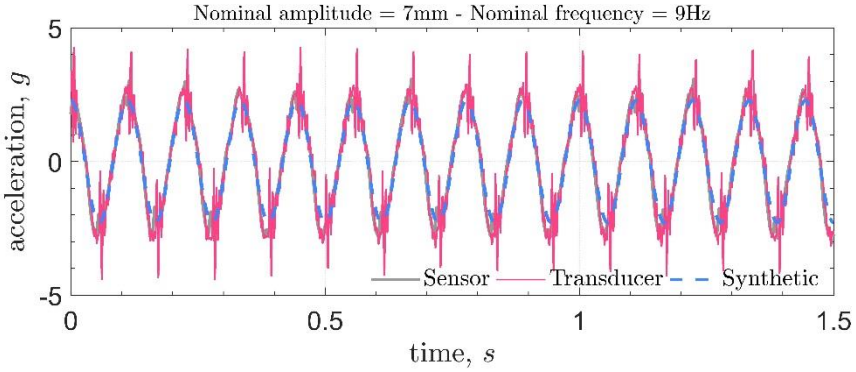

(B6)

Appendix C: Data used for spectral amplitude method (selected)

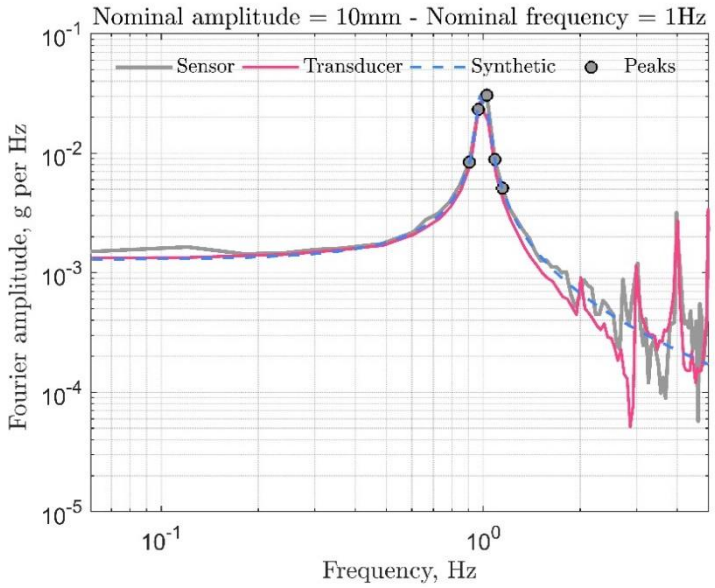
Nominal amplitude = 10mm - Nominal frequency = 1Hz
Sensor
Transducer
Synthetic
Peaks
Fourier amplitude, g per Hz
Frequency, Hz

(C1)

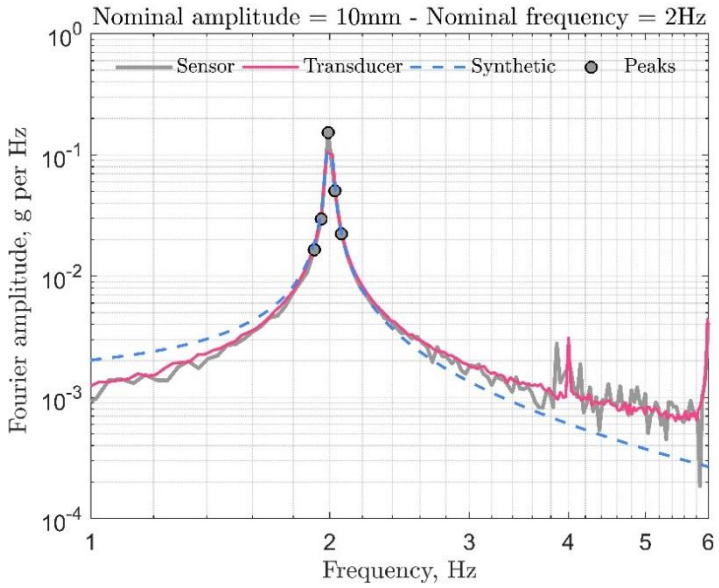
Nominal amplitude = 10mm - Nominal frequency = 2Hz
Sensor
Transducer
Synthetic
Peaks
Fourier amplitude, g per Hz
Frequency, Hz

(C2)

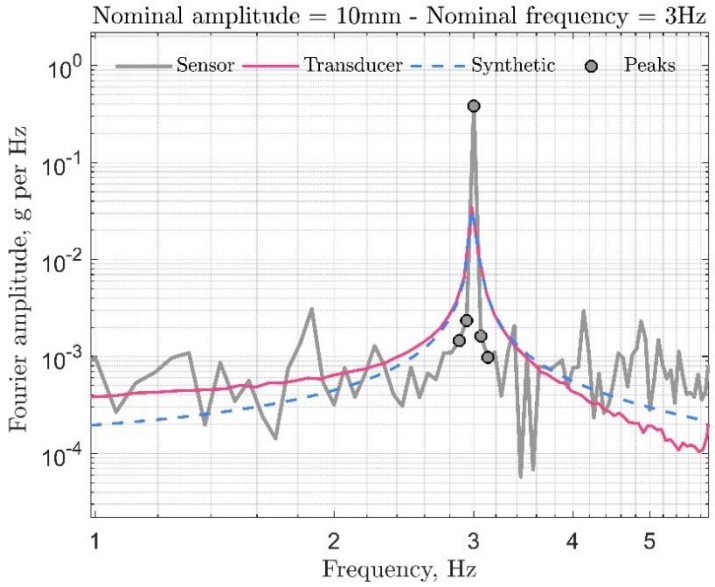
Nominal amplitude = 10mm - Nominal frequency = 3Hz
Sensor
Transducer
Synthetic
Peaks
Fourier amplitude, g per Hz
Frequency, Hz

(C3)

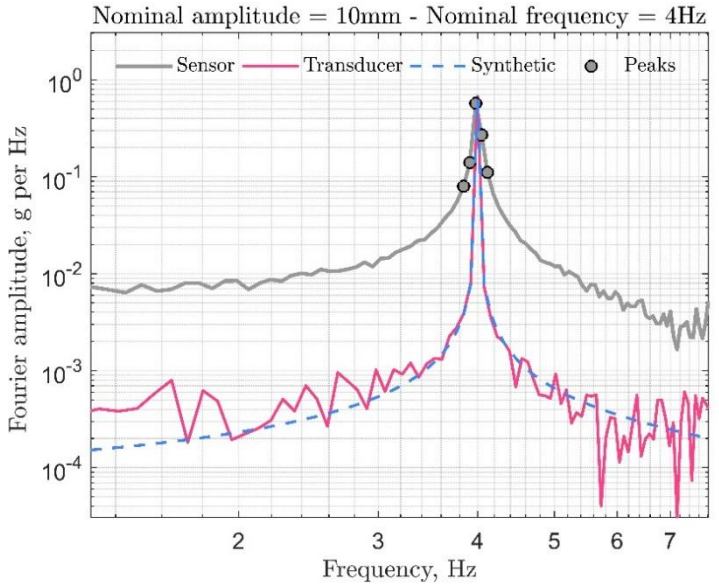
Nominal amplitude = 10mm - Nominal frequency = 4Hz
Sensor
Transducer
Synthetic
Peaks
Fourier amplitude, g per Hz
Frequency, Hz

(C4)

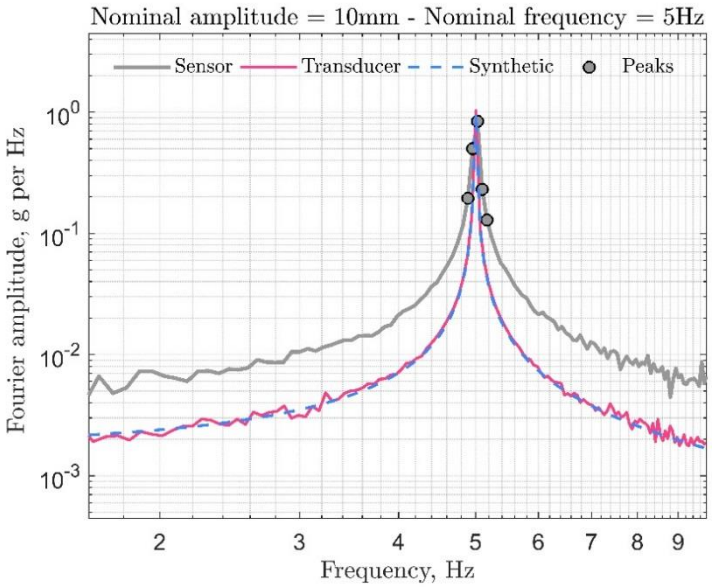
Nominal amplitude = 10mm - Nominal frequency = 5Hz
Sensor
Transducer
Synthetic
Peaks
Fourier amplitude, g per Hz
Frequency, Hz

(C5)

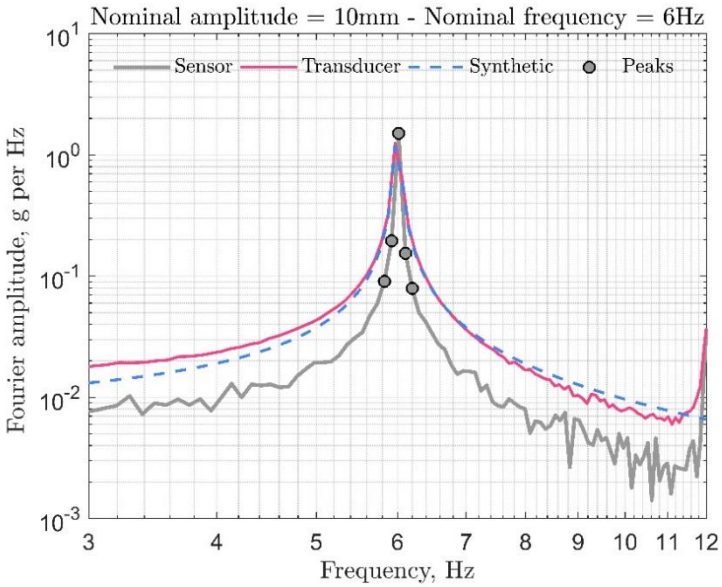
Nominal amplitude = 10mm - Nominal frequency = 6Hz
Sensor
Transducer
Synthetic
Peaks
Fourier amplitude, g per Hz
Frequency, Hz

(C6)

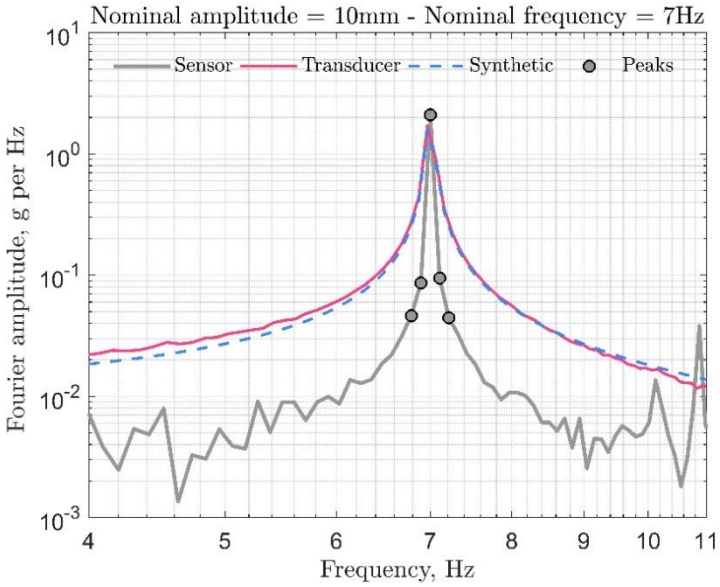
Nominal amplitude = 10mm - Nominal frequency = 7Hz
Sensor
Transducer
Synthetic
Peaks
Fourier amplitude, g per Hz
Frequency, Hz

(C7)

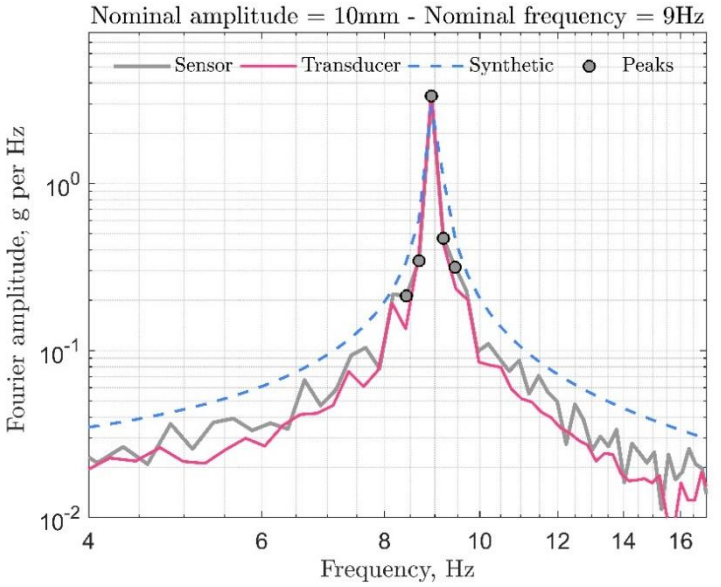
Nominal amplitude = 10mm - Nominal frequency = 9Hz
Sensor
Transducer
Synthetic
Peaks
Fourier amplitude, g per Hz
Frequency, Hz

(C8)

Appendix D: Data used for single and double-integration test (selected)

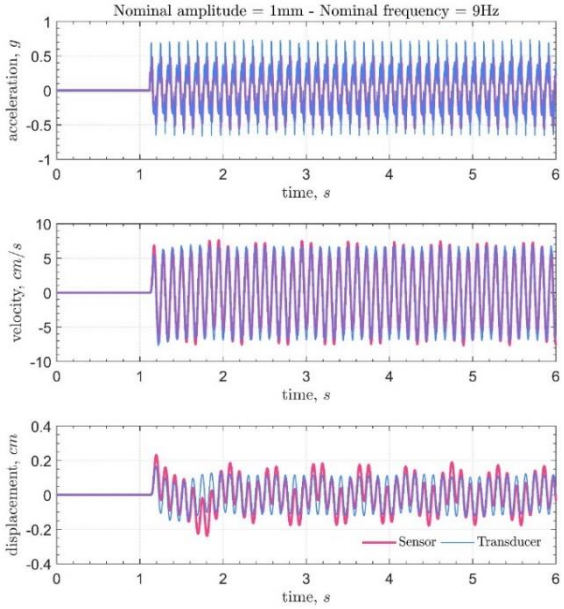
Nominal amplitude = 1mm - Nominal frequency = 9Hz
acceleration, g
time, s
velocity, cm/s
time, s
displacement, cm
Sensor
Transducer
time, s

(D1)

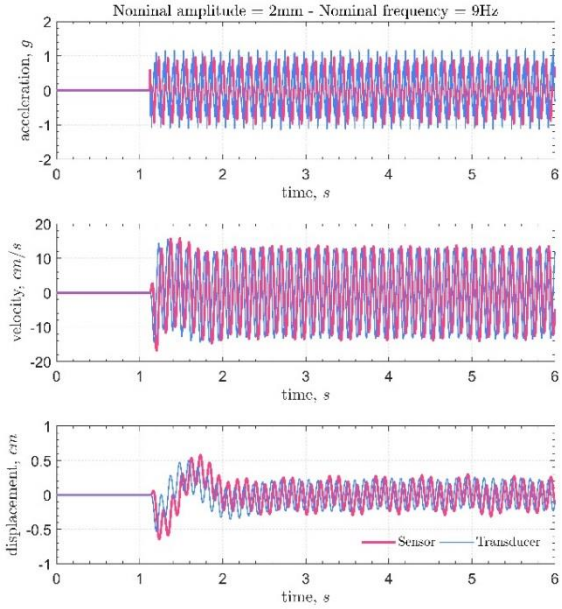
Nominal amplitude = 2mm - Nominal frequency = 9Hz
acceleration, g
time, s
velocity, cm/s
time, s
displacement, cm
Sensor
Transducer
time, s

(D2)

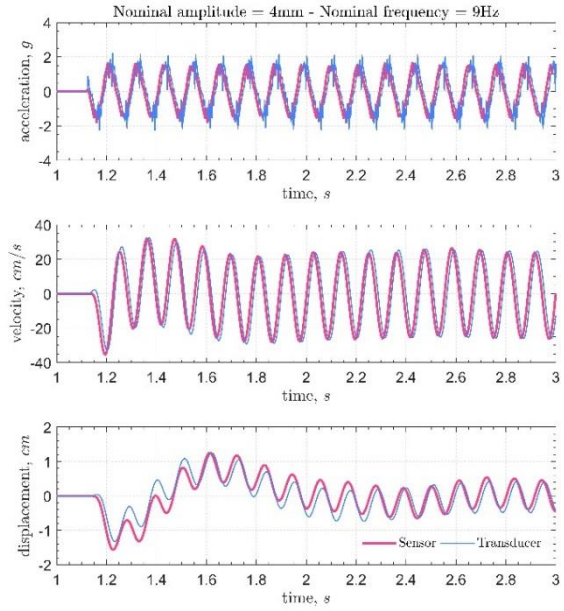
Nominal amplitude = 4mm - Nominal frequency = 9Hz
acceleration, g
time, s
velocity, cm/s
time, s
displacement, cm
Sensor
Transducer
time, s

(D3)

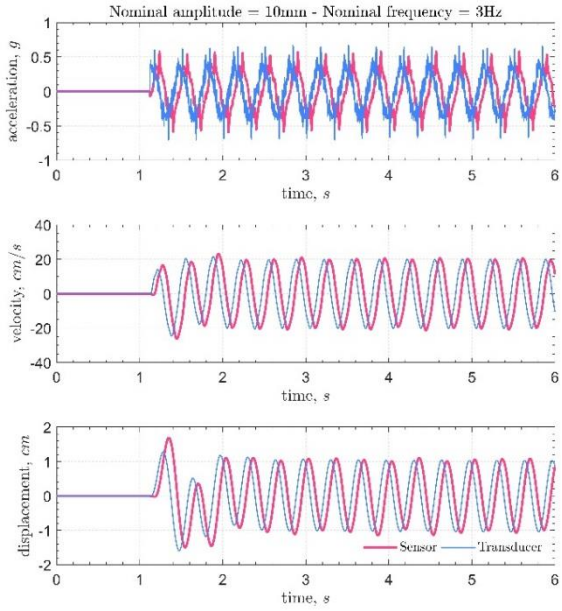
Nominal amplitude = 10mm - Nominal frequency = 3Hz
acceleration, g
time, s
velocity, cm/s
time, s
displacement, cm
Sensor
Transducer
time, s

(D4)